ISSN1346-7832

独立行政法人港湾空港技術研究所

港湾空港技術研究所報告

REPORT OF THE PORT AND AIRPORT RESEARCH INSTITUTE

VOL.42 NO.2 June 2003

NAGASE,YOKOSUKA,JAPAN
INDEPENDENT ADMINISTRATIVE INSTITUTION,
PORT AND AIRPORT RESEARCH INSTITUTE

港湾空港技術研究所報告（REPORT OF PARI）
第42巻　第2号（Vol. 42, No. 2），2003年6月（June 2003）

目　　次（CONTENTS）

TECHNICAL REPORT OF THE PORT AND
AIRPORT RESEARCH INSTITUTE
Vol. 42, No. 2, June 2003.

Concrete Properties and Relationship Between Surface Strain and Strain Over the Steel Bars of ASR Affected Concrete Members

Tarek Uddin MOHAMMED*

Hidenori HAMADA**

Toru YAMAJI***

Synopsis

A detailed experimental investigation was carried out to understand the change in mechanical properties of concrete, surface strain over the specimens and the steel bars embedded in concrete, crack growth, and change in mechanical properties of steel bars under sustained stress induced by the alkali-silica reaction (ASR) in concrete. Also, chloride diffusion in concrete, corrosion over the steel bars, investigation on ASR gel at the porous matrix region by SEM, and visual examination of the ASR gel on the cut surface of the specimens were carried out. For this, beam specimens of size $250 \times 250 \times 600$ mm and cylinder specimens of diameter 100 mm and length 200 mm were made. Beam specimens were made with and without reinforcements. Various restrained conditions by the reinforcement were provided. Additional NaOH was added to raise the total Na_2O equivalent alkali content to 6 kg/m^3 in concrete. The specimens were submerged in seawater at a temperature of 40°C in a closed container. The investigation was carried out for 383 days.

Young's modulus of concrete drops significantly due to ASR immediately after cracking, but later stabilizes. The reduction in compressive strength was not as significant as that of Young's modulus. Internal restraint provided by the steel bars results in the reduction of surface strain in the restraint direction. The degree of restraint has a significant influence on the surface strain as well as the strain over the steel bars. A good linear relationship between the surface strain and the strain over the steel bars is found, especially for the cases with highly restrained conditions. Less surface strain is observed if the steel bars are placed near the concrete surface, however, the strain over the bars is increased for this arrangement. Placing of longitudinal steel bars near the surface also results in the significant lateral surface strain as well as higher strain over the stirrups, if any.

Key Words: alkali-silica reaction, concrete, steel bar, strain.

* Research Engineer (Senior), Materials Division, Geotechnical and Structural Engineering Department
** Chief Research Engineer, Materials Division, Geotechnical and Structural Engineering Department
*** Research Engineer, Materials Division, Geotechnical and Structural Engineering Department
3-1-1 Nagase, Yokosuka, 239-0826 Japan.
Phone : +81-468-44-5061 Fax : +81-468-44-0255 e-mail : tarek@pari.go.jp

港湾空港技術研究所報告
第 42 巻第 2 号(2003.6)

ASR が発生したコンクリートの特性および内部鉄筋ひずみとコンクリート表面ひずみの関係

タレク　ウディン　モハメッド*・濵田　秀則**・山路　徹***

要　旨

アルカリ骨材反応（ASR）が発生しているコンクリートにおいて生じている，コンクリート自身の物性，内部鉄筋およびコンクリート表面のひずみ，ひび割れの進展，鉄筋の機械的性質等の変化に関して詳細な実験的検討を行った．それに加えて，コンクリート中への塩化物イオンの拡散性状の試験，内部鉄筋の腐食状況の観察，SEM によるアルカリシリカゲルの観察，コンクリートの破断面におけるアルカリシリカゲルの観察を行った．実験には，寸法が 250×250×600mm の角柱型の供試体，および直径が 100mm，長さが 200mm の円柱型の供試体を用いた．角柱型供試体には鉄筋コンクリート製と無筋コンクリート製の 2 種類があり，鉄筋コンクリート製の場合には，鉄筋量を数種に変えることにより，数種の異なる拘束状態に設定した．また，コンクリート中のアルカリ総量を等価 Na_2O で 6 kg/m^3 になるように，練り混ぜ自に NaOH を加えている．供試体は，40℃に加熱した海水中に浸せきした．この状態で最長 383 日まで養生を行い，その間およびその後に各種の試験を実施した．

コンクリート表面にひび割れが発生した直後，コンクリートの弾性係数は大幅な低下を示したが，その後はほぼ定常状態となった．コンクリートの圧縮強度の低下は，弾性係数の低下ほど顕著には生じなかった．内部鉄筋の有する拘束効果により，コンクリートの表面ひずみは抑制されていた．内部鉄筋の拘束率は，コンクリート表面のひずみおよび鉄筋のひずみに大きく影響していた．コンクリート表面のひずみと内部鉄筋のひずみには線形の関係が認められ，かつそれは鉄筋による拘束率が大きくなるほど相関性が高くなった．内部鉄筋がコンクリート表面に近いほどコンクリート表面のひずみは小さくなる傾向にあるが，鉄筋のひずみは大きくなる傾向にあった．コンクリート表面近傍に縦断方向の鉄筋を配置した場合は，横方向のコンクリート表面ひずみおよびスターラップ鉄筋のひずみが大きくなった．

キーワード：アルカリ骨材反応，コンクリート，鉄筋，ひずみ

*　地盤・構造部　材料研究室　研究官（シニア）
**　地盤・構造部　材料研究室　室長
***　地盤・構造部　構造強度研究室　研究官
〒239－0826　神奈川県横須賀市長瀬 3－1－1　独立行政法人港湾空港技術研究所
TEL：0468－44－5061　FAX：0468－44－0255　e－mail：tarek@pari.go.jp

Contents

1. Introduction

Alkali-silica reaction (ASR) occurs between the reactive silica in aggregate and the alkali solution in concrete. The reaction produces a gel that absorbs water and consequently expands. The gel restrained to spread freely into the concrete at the initial stage. As a result, tensile stress is built up locally and cracking occurs when the pressure generated at localized sites of expansive reaction exceeds the tensile strength of concrete. In the last couple of decades numerous studies were carried out to understand the reaction mechanism associated with ASR in concrete, the mineral components in aggregates causing the reaction, the factors controlling the reaction, stress induced in the steel bars due to this reaction, the size effect of the specimens on the expansion, the influence of the steel ratio in the specimens, the fatigue behavior of the concrete beams subjected to ASR, the ways to rehabilitate the damaged concrete structures caused by this reaction, and development of the specifications to avoid the occurrence of ASR (**1~14**). Nevertheless, studies on the strain induced over the concrete surface as well as the steel bars are still necessary with various restrained conditions provided by the embedded steel bars inside concrete. This kind of study is also recommended by ACI (**15**). Also, with the existence of relations between the surface strain and the strain over the steel bars due to ASR, engineers can predict the strain over the steel bars from the measured surface strain. Unfortunately, this kind of study is very rare in the technical literature due to the difficulties in continuous measurement of steel strain inside the specimens.

With the above-mentioned background, a detailed experimental study was carried out on plain and reinforced concrete beam specimens of size $250 \times 250 \times 600$ mm to investigate the ASR induced surface strain over the concrete surface as well as the strains over the steel bars embedded in concrete. Cylinder specimens were also investigated for the evaluation of variations in pulse velocity, compressive strength, and Young's modulus of concrete with the progress of ASR in concrete. The study was continued until 383 days. Empirical relationships between the surface strain and strain over the steel bars were proposed for different restrained conditions. Moreover, the change in mechanical properties of the steel bars after sustained loading due to ASR, corrosion of steel bars in concrete, chloride diffusion, SEM investigation of ASR gel, microstructure of concrete in the inner and outer regions, crack patterns, depth of cracks, and the condition of the cut surface of the beam specimens were also reported in this paper. An intermediate report of this study was submitted explaining the data till the age of 198 days (**16**).

Table 1 Physical and Chemical Compositions of Cements

Specific Gravity	3.16
Blaine Fineness, cm^2/g	3190
Ignition Loss, %	0.7
SiO_2, %	21.3
Al_2O_3, %	5.3
CaO, %	64.4
MgO, %	2.2
SO_3, %	1.9
Fe_2O_3, %	2.6
Na_2O Equiv., %	0.65

Table 2 Properties of the Aggregates

Aggregate	Specific Gravity	Water Absorption (%)	FM
Reactive Coarse Aggregate	2.63	0.62	6.61
Non-Reactive Coarse Aggregate	2.64	0.76	6.67
Fine Aggregate	2.6	2.32	2.91

Table 3 Mechanical Properties of the Steel Bars

Items	Round Bar (13mm)	Deformed Bar (12.7mm)	Round Bar (25mm)	Round Bar (6mm)
Yield Stress (MPa)	373	387	370	299
Young's Modulus ($\times 10^5$ MPa)	2.03	1.80	2.11	1.96
Yield Strain ($\mu\varepsilon$)	1837	2150	1750	1525
Ultimate Stress(MPa)	547	565	561	489
Elongation (%)	23	20	25	21

Table 4 Mixture Proportions of Concrete

	Normal Concrete	ASR Concrete
G_{max} (mm)	20	20
Slump (cm)	11±1	11±1
Air (%)	4±1	4±1
W/C (%)	47	47
S/a (%)	41	41
W (kg/m^3)	170	170
C (kg/m^3)	362	362
S (kg/m^3)	720	720
G (kg/m^3)	1051	1047
AEWRA (kg/m^3)	0.905	0.905
AEA (g/m^3)	3.62	3.62
NaOH (kg/m3)	-	4.7

W, C, G, and S refer respectively to water, cement, gravel and sand. s/a is the sand-aggregate ratio. AEA and AEWRA mean air-entraining, and air-entraining water-reducing admixtures, respectively.

2. Experimentation

2.1 Scope

Cylinder (diameter 100 mm and length 200 mm) and beam specimens (250 × 250 × 600 mm) were investigated. The specimens were made with ordinary portland cement (OPC). Additional alkali was added to raise the Na_2O equivalent alkali content in concrete to 6 kg/m^3 (1.67% of cement mass). W/C was 0.47. The specimens were submerged in 40°C seawater in a closed container. Different internal restraints were provided by the various layout of the steel bars embedded in the concrete beams. The surface strains and crack maps over the specimens were measured periodically. Strain over the steel bars was recorded automatically through a data logger. In addition, cylinder specimens 100 mm in diameter and 200 mm in length were also periodically tested for pulse velocity, compressive strength, and Young's modulus. These investigations were carried out until 383 days of exposure. At 303 days of exposure, chloride ingress, corrosion of steel bars, microstructure of the inner and outer regions ((by Scanning Electron Microscope (SEM) and Mercury Intrusion Porosimeter (MIP)) of the specimens were also investigated. Moreover the condition of the internal portion of the beam specimens was checked after cutting the specimens at the same exposure period.

2.2 Materials

Ordinary portland cement (OPC) was used. The physical properties and chemical analysis are shown in **Table 1**. Additional NaOH was added to raise the Na_2O equivalent alkali content in concrete to 6 kg/m^3.

Crushed reactive (chert) and non-reactive (granite) coarse aggregates were used. In the case of ASR specimens, only the reactive coarse aggregates were used. The sand was non reactive. The properties of reactive and non-reactive aggregates are shown in **Table 2**. The reactivity of the coarse aggregates was confirmed by concrete prism tests before making the specimens as per ASTM C1293. Japanese Industrial Standard round (SR295) and deformed (SD295A) steel bars were used. The mechanical properties of the steel bars measured at the laboratory are listed in **Table 3**. The size of the end steel plates was 50 × 50 × 6 mm (SS 400). The end plates were rigidly welded with the steel bars. Type FLA-3-11-5LT (Three wire type, Gauge length = 3 mm, and Gauge resistance = 120 ohm, Temperature compensation range = 10 to 80°C, Material = Cu-Ni, Base = Epoxy, Wire Length=5 mm) and Type FLK-2-11-5LT (Gauge Length = 2 mm, all others same as before) strain gauges were used to measure strain over the main steel bars and stirrups, respectively.

2.3 Mixture Proportions

Mixture proportions of concrete are summarized in **Table 4**. W/C was 0.47. The slump of the fresh concrete was 11±1 cm and air content 4±1 %. Both air entraining and air entraining water reducing agents were used. Mixing water was tap water.

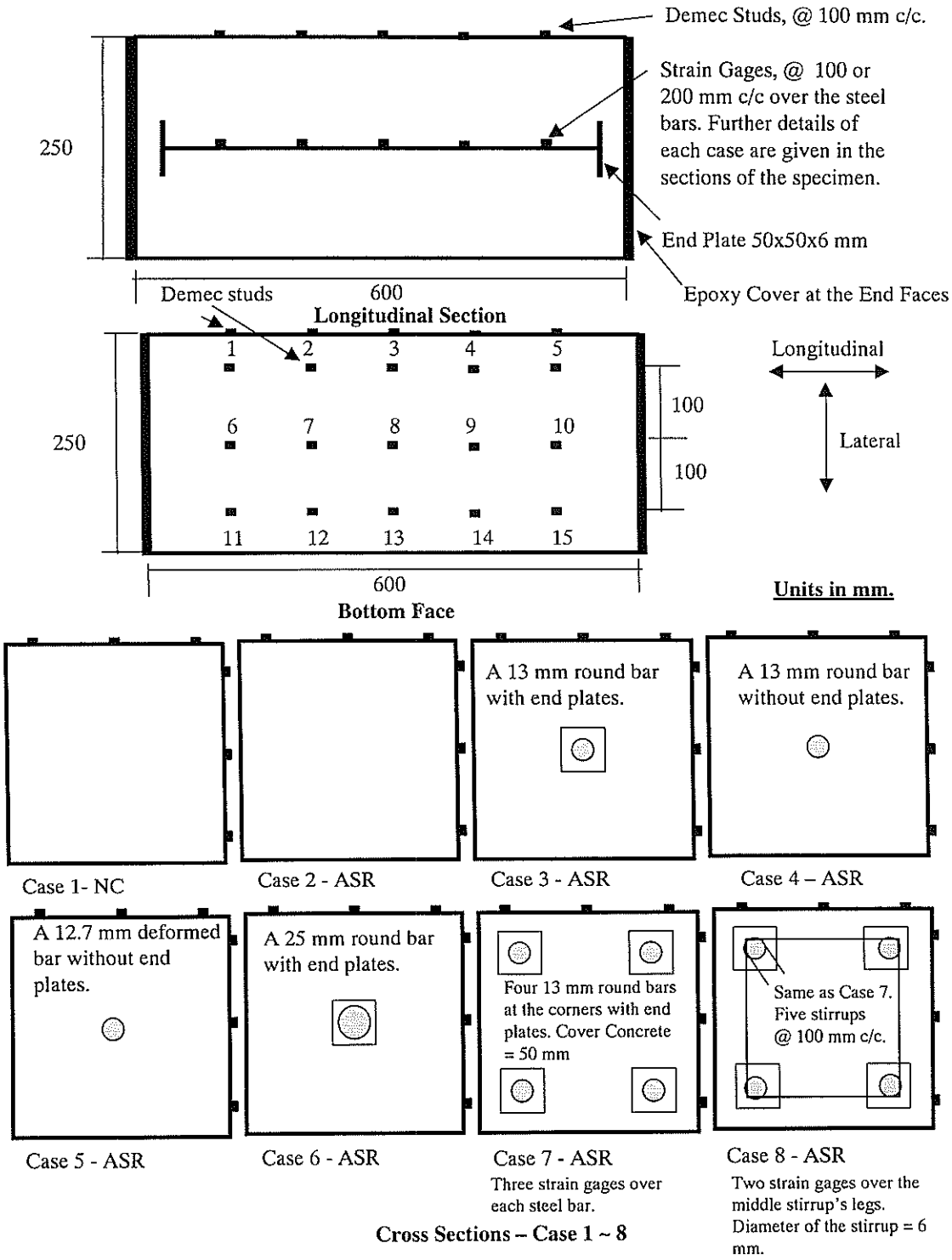

Fig. 1 Layout of the Specimens

Table 5 Physical Properties and Chemical Composition of Seawater

Specific Gravity	pH	Na ppm	K ppm	Ca ppm	Mg ppm	Cl ppm	SO_4 ppm	CO_3 ppm
1.022	7.77	9290	346	356	1167	17087	2378	110

All strain gages are connected with data logger and two switch boxes.

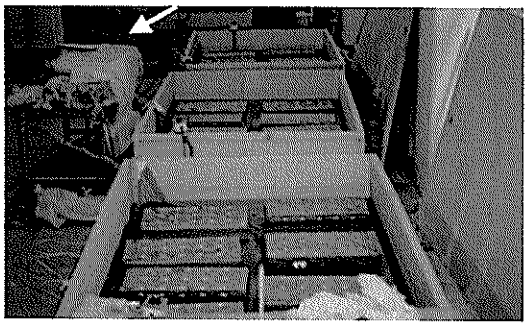

The specimens are supported on three plastic rollers to avoid friction at the base. The side face with stud gages is kept top.

Fig. 2 A View of the Specimens

2.4 Specimens and Method of Evaluation

Plain and reinforced concrete prism specimens of size $250 \times 250 \times 600$ mm were made as shown in **Fig. 1** with and without reactive coarse aggregates and other variables mentioned earlier. Eight separate cases were made. The cross sections of all cases are given in **Fig. 1**. A view of the specimens is shown in **Fig. 2**. A brief explanation of the cases (C1~C8) investigated in this study is given below:

Case 1 Normal concrete (made with non-reactive aggregate) without reinforcement.
Case 2 ASR Concrete without reinforcement.
Case 3 ASR concrete. A 13 mm round bar was embedded at the center with end plates.
Case 4 ASR concrete. A 13 mm round bar was embedded at the center without end plates.
Case 5 ASR concrete. A 12.7 mm deformed bar was embedded at the center without end plates.
Case 6 ASR concrete. A 25 mm round bar was embedded at the center with end plates.
Case 7 ASR concrete. Four 13 mm round bars were embedded at the corners with end plates.
Case 8 ASR concrete. Four 13 mm round bars were embedded at the corners with end plates. In addition, five stirrups (round bar, 6 mm diameter) were embedded @ 100 mm c/c.

The end plates were used to consider the effect of the bar with end anchorage. The presence of end plates also confine the concrete surrounding the steel bars enclosed by the end plates. Therefore it is expected that for these cases (Case 3, Cases 6~8), the influence of type of bars (plain or deformed) will be negligible.

For Case 1, two specimens were made. For all other cases, three specimens per each case were made. Demec studs were placed over the concrete surface @ 100 mm c/c in both lateral and longitudinal directions as shown in **Fig. 1**. They were placed on the bottom face (opposite to the finishing face after casting concrete) and one side face of the specimens. Here, the results on the side face are only explained. Five strain gages were fastened over the steel bars @ 100 mm c/c for Cases 3~6. For Cases 7 and 8, three strain gages were fastened @ 200 mm c/c over each steel bar. For Case 8, in addition to strain gages over longitudinal steel bars, two strain gages were fastened over the mid stirrup, one at the vertical leg and one at the horizontal leg. To fasten the strain gauge, a smooth surface was prepared over the steel bars and the strain gauges were glued over it and covered with adhesive tape. All strain gages were connected with a data logger. Two switch boxes were also connected with the data logger for the automatic recording of all strains (total 138 locations) over the steel bars concurrently once in a day.

After 28 days of standard curing, the demec studs were fastened over the concrete surface and at the age of about 45 days the specimens were transferred to the exposure tanks. Three wooden tanks were specially fabricated for this purpose. The specimens were rested on three plastic pipes (diameter 3 cm) glued over the bottom face of the tank. This was done to reduce the friction at the contact surfaces. The specimens were submerged in seawater directly supplied from the sea. The physical properties and chemical composition of seawater are listed in **Table 5**. The temperature of seawater was controlled at around 40°C. One heater was placed in each tank and the water was continuously circulated through a pump to maintain a uniform temperature in the tank. The tanks were covered during exposure.

Strain over the steel bars was measured once in a day through the data logger automatically. Some of the strain gages became inactive after cracking of the specimens. The average of all strain measured over the steel bars for each specimen is reported as the representative strain for the specimen. The change in length between the demec studs was measured by a digital extensometer periodically. The side face with demec studs kept top in the tank for easy measurements of length change during exposure. The average of all

measured longitudinal strains is defined as longitudinal strain for each specimen. In the same way, the average of all lateral strains is defined as the lateral strain. Cracks were marked over the specimens periodically and photographs were taken. Large crack widths were also measured. The measurements were taken just after removing a portion of water from the tank so that the measurement of length between the demec studs is possible. The tank was filled and covered soon after all measurements, such as change in length between the demec studs, recording of the large crack widths and marking the cracks, and taking photographs.

In addition to the prism specimens, cylinder specimens (12 specimens with non-reactive aggregate and 36 specimens with reactive aggregate) of 100 mm in diameter and 200 mm in length were also made. The specimens were exposed in the tank with the prism specimens. The specimens were periodically tested for pulse velocity, compressive strength, and Young's modulus. Before measurements, the specimens to be tested were transferred in a controlled room of temperature about 20°C and relative humidity more than 80%. The specimens were also kept covered with wet cloths to avoid moisture loss from the specimens.

After 303 days of continuous exposure, one specimens from each case (Case 2~8) was cut to collect the steel bars as well as to see the internal condition of the specimens, the crack depths, corrosion over the steel bars. In addition, samples were also carefully collected to measure the porosity of the mortar portions at the inner and outer regions, SEM evaluation of the dense matrix, porous matrix, and entrained air voids. Mechanical properties of the steel bars were also tested.

3. Experimental Results and Discussion

The results of this study are explained in six subsections, titled "Pulse Velocity, Compressive-Strength and Young's Modulus", "Longitudinal and Lateral Strains Over the Concrete Surface", "Strain Over the Steel Bars Embedded in Concrete", "Crack Maps, Carck Intensity, Crack widths and Depths, and Overall Volume Expansion", "Relationships Between Surface Strain and Strain Over the Steel Bars", and "Others". "Others" includes chloride diffusion, corrosion over the steel bars, mechanical properties of steel bars, microstructure of concrete, condition of the inner regions of the specimens, and crack depths at 303 days of exposure.

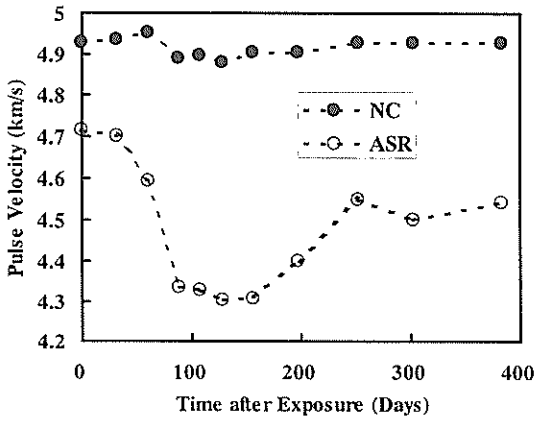

Fig. 3 Pulse Velocity Through Concrete

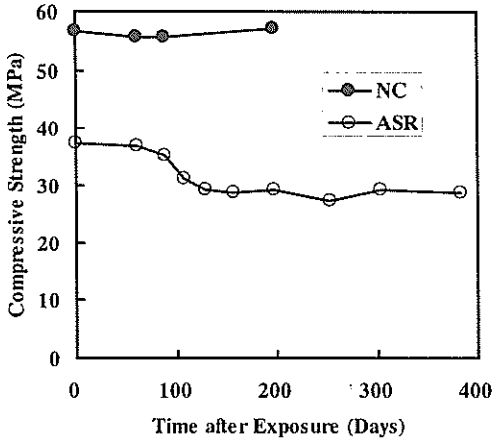

Fig. 4 Compressive Strength of Concrete

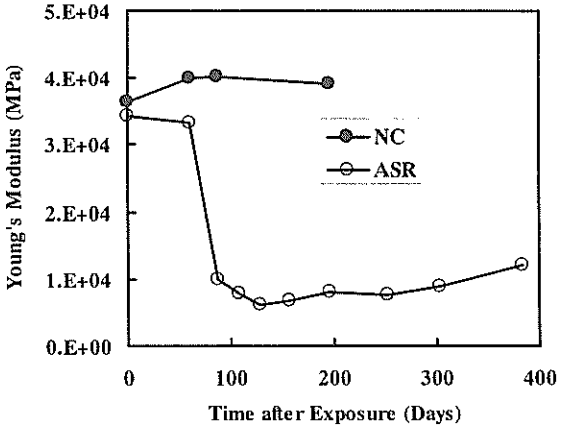

Fig. 5 Young's Modulus of Concrete

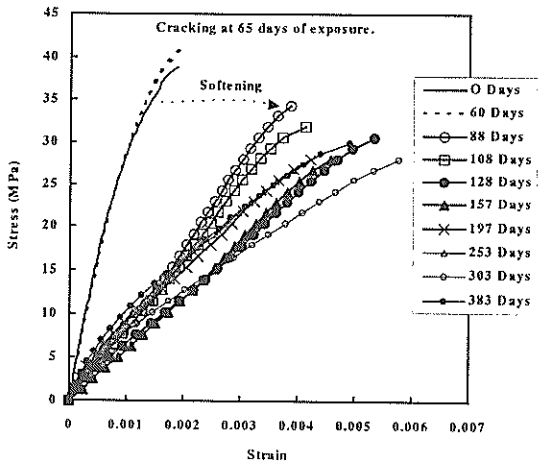

Fig. 6 Stress-Strain Curves of ASR Concrete

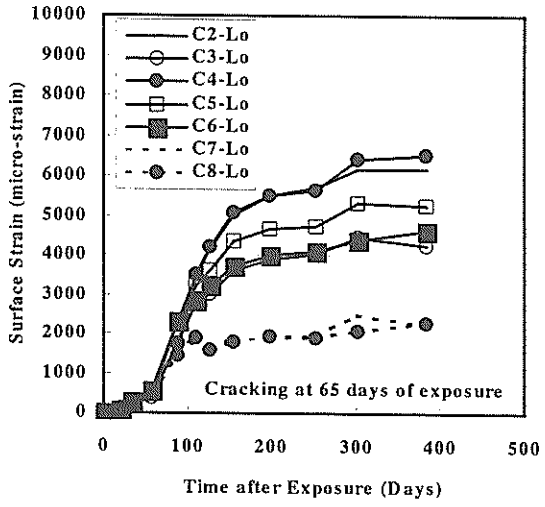

Fig. 7 Longitudinal Surface Strain (Lo) Over the Specimens

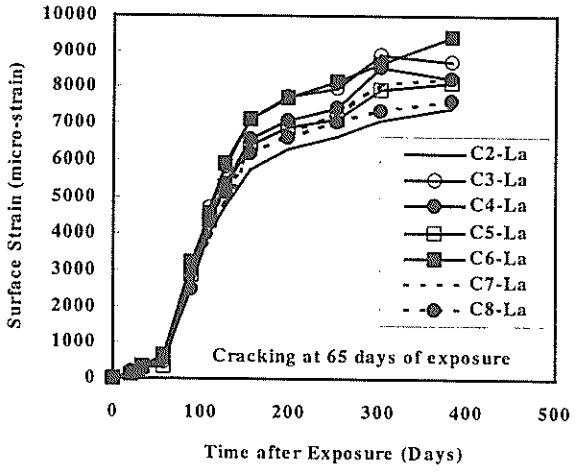

Fig. 8 Lateral Surface Strain (La) Over the Specimens

3.1 Pulse Velocity, Compressive Strength, and Young's Modulus

The variations of the ultrasonic pulse velocity, compressive strength, and Young's modulus with the exposure period are shown in **Figs. 3~5**. The pulse velocity decreases gradually during the early age of exposure. It quickly drops after cracking around 65 days of exposure. Later it increases slightly and reaches a constant value without decreasing further due to the healing of voids and cracks by ASR gel. Visual observation of the cut surface and SEM photos of the fractured surface are explained later. The compressive strength is slightly reduced at the early age of exposure. The reduction is relatively more immediately after cracking at 65 days of exposure. However, no significant reduction is observed later, i.e., a stable value is reached. The lower strength of ASR specimens compared to the specimens made with non-reactive aggregate cannot be explained here, as no specimens were tested for normal concrete with the additional alkali. The Young's modulus gradually decreases at the early age of exposure and quickly drops after cracking, and finally becomes almost stable. The change in Young's modulus is more significant than any other changes explained earlier, such as pulse velocity and compressive strength. Typical stress-strain curves of the cylinder specimens are shown in **Fig. 6** at the different exposure periods until the age of 383 days. Significant softening is observed due to the ASR expansion, especially immediately after cracking at 65 days of exposure. No further softening is observed at the later age of exposure. The significant reduction in Young's modulus of concrete due to ASR at the early stage of exposure is also reported in other references (**1,16**). It is explained due to the generation of micro cracking in concrete due to the ASR.

From the above-mentioned results, ASR induced expansion is divided into three periods, such as the incubation period, cracking period, and stabilized period. In the incubation period, the change in properties is slow, in the cracking period the change is very fast, and in the stabilized period no significant change is found.

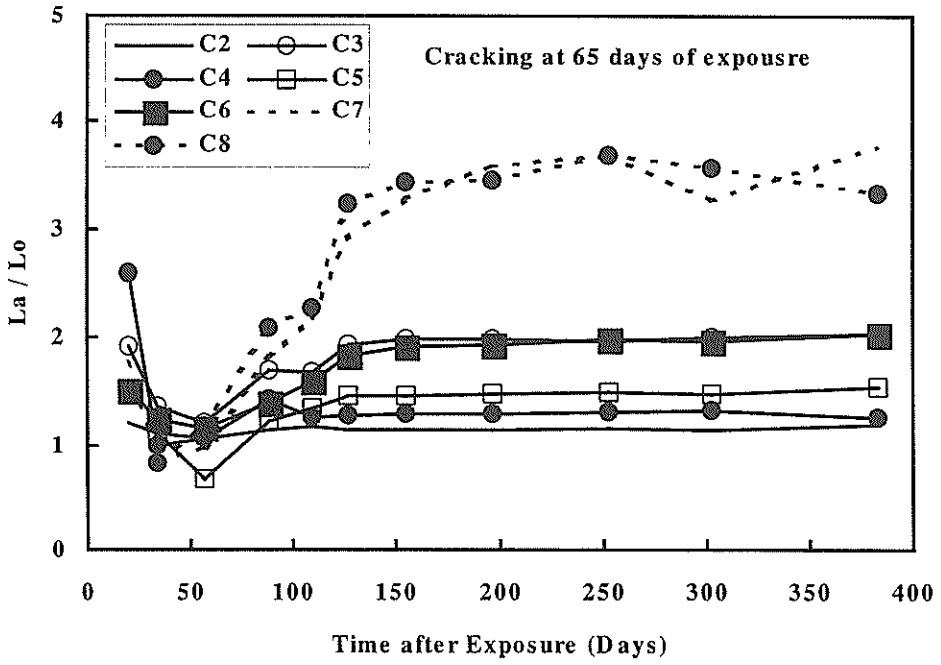

Fig. 9 The Ratio of Lateral Strain (La) to Longitudinal Strain (Lo)

3.2 Longitudinal and Lateral Strains Over the Concrete Surface

Longitudinal and lateral strains over the specimens were calculated based on the measured surface strains over the specimens by using the following equations:

Longitudinal Strain

$$\varepsilon_{lo} = \frac{\sum_{i=1}^{4} \varepsilon_{i,i+1} + \sum_{i=6}^{9} \varepsilon_{i,i+1} + \sum_{i=11}^{14} \varepsilon_{i,i+1}}{12} \quad (1)$$

Lateral Strain

$$\varepsilon_{la} = \frac{\sum_{i=1}^{10} \varepsilon_{i,i+5}}{10} \quad (2)$$

Where, $\varepsilon_{i,j}$ is strain between studs i and j (**Fig. 1**).

For Case 1, the surface strain was lower than 200 $\mu\varepsilon$ after 383 days of exposure and also no cracks were found over the specimens. The longitudinal and lateral strains over the specimens for Cases 2~8 are shown in **Figs. 7** and **8**. The ratios of lateral to longitudinal surface strain are shown in **Fig. 9**. The results of each individual specimen of each case until the age of 198 days were reported in **Reference 16**. Almost similar results were observed between the specimens of each case. Irrespective of the cases, no significant difference in strain is observed at the early stage of exposure. However, after cracking at 65 days of exposure, a significant difference in longitudinal strain is observed depending on the restraint provided by the steel bars inside the specimens. Irrespective of the cases, it is also found that strain increases gradually and becomes almost stable later. The other results related to each case are explained below:

Case 2

This is the ASR case without reinforcement. A significant amount of lateral and longitudinal strains are observed at the age of 383 days (**Figs. 7** and **8**). The lateral strain in the longitudinal direction exceeds 6000 $\mu\varepsilon$ (0.6%) at 383 days of exposure. The lateral strain exceeds 7000 $\mu\varepsilon$ (0.7%) at the same exposure period. As no steel bar was embedded in this case, therefore, the specimens were free to expand in both lateral and longitudinal directions. The ratio of the lateral to longitudinal strains is close to unity, which indicates almost equal strain in lateral and longitudinal directions (**Fig. 9**).

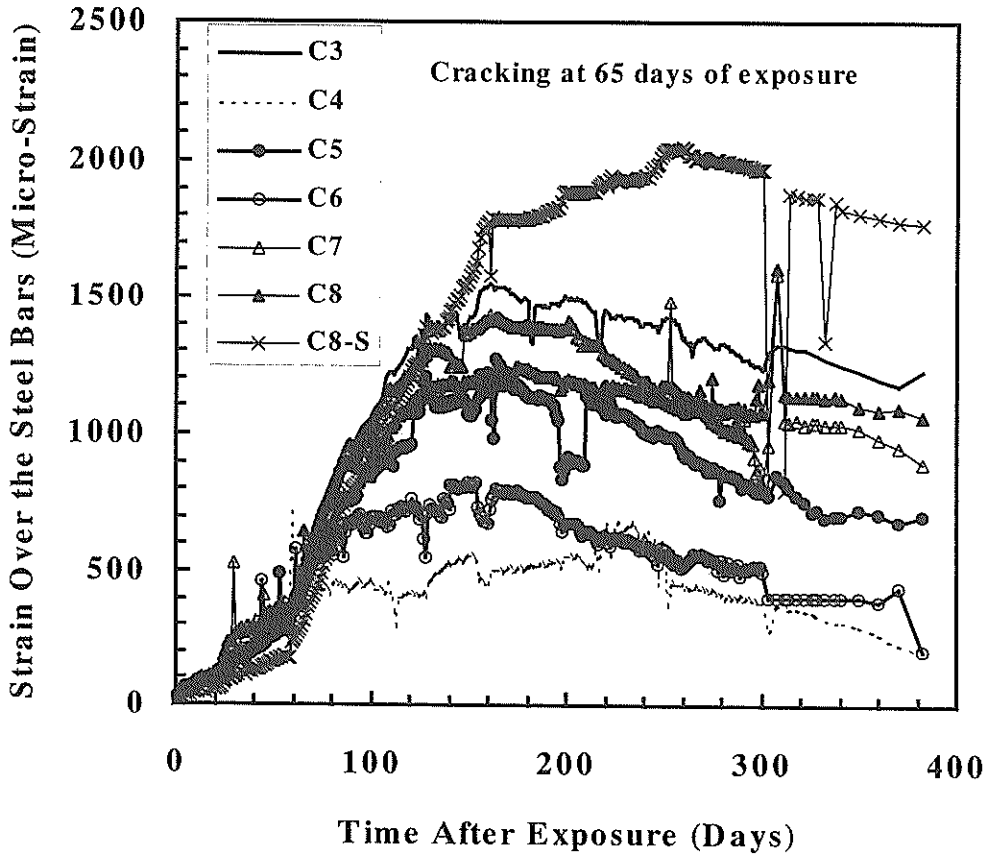

Fig. 10 Strain Over the Steel Bars

Case 3

This is the ASR case with a 13 mm steel bar at the center with end plates. A clear difference between the longitudinal and lateral strains is observed after cracking of the specimens. The restraint in the longitudinal direction provided by the steel bars with end plates reduces the surface strain over the specimens in the longitudinal direction. The lateral and longitudinal strains are around 9000 and 4000 $\mu\varepsilon$, respectively at 383 days. The ratio of the lateral to longitudinal strains almost stabilized at around 2. Comparing Cases 2 and 3, the change in the strains due to the restraint can be clearly realized after cracking of the specimens.

Case 4

In this ASR case, a 13 mm round bar was embedded at the center of the specimen without end plates. Removal of the end plates from the end of the bar reduces the degree of restraint in the longitudinal direction compared to Case 3. The strains in the lateral and longitudinal directions become about 8000 $\mu\varepsilon$ and 6500 $\mu\varepsilon$, respectively. The surface strains were very similar to Case 2, i.e., the case without reinforcement. The results indicate that a little restraint is provided by the embedded steel bar for Case 4. The ratio of the lateral to longitudinal strains is stabilized at around 1.3 (**Fig. 9**). The higher value of lateral to longitudinal strain at the early age of exposure is expected due to the error in measurements of a very small strain over the specimen.

Case 5

In this ASR case, to increase the degree of restraint compared to Case 4, a deformed bar of diameter 12.7 mm was embedded at the center of the specimens. The lateral and longitudinal strains become 5500 $\mu\varepsilon$ and 8000 $\mu\varepsilon$, respectively. Same as before, the

longitudinal restraint provided by the steel bar in concrete results in the reduction in longitudinal strains compared to the lateral strains. However, this reduction is more than Case 4, i.e., the case with a plain bar without end plates, but less than the Case 3, i.e. the case with a plain bar with plates at the ends. In Case 5, the degree of restraint is higher compared to Case 4, but lower compared to Case 3. The results strongly suggest that the degree of the restraint has a significant influence on the strain over the concrete surface. The ratio of the lateral to longitudinal strains is stabilized at around 1.5, which is higher than Cases 2 and 4, but lower than Case 3 (**Fig. 9**).

Case 6

In this ASR case, a 25 mm bar was embedded at the center with end plates. The steel area is about 3.7 times higher than Case 3. After cracking of the specimens, a clear difference between the lateral and longitudinal strains is observed as in Case 3. No remarkable difference between the lateral and longitudinal strains is observed between Case 6 and Case 3. The ratio of the lateral to longitudinal strain is stabilized at around 1.9, which is slightly lower than Case 3 (**Fig. 9**). No significant difference in the surface strains of Case 3 and Case 6 indicates that both cases are providing the same amount of restraint. However, strain over the steel bars was lower for Case 6 compared to Case 3. These data are explained later.

Case 7

In this ASR case, four 13 mm steel bars were provided with end plates. The total area of the steel bar was similar to Case 6. For Case 7, a significant reduction in the longitudinal strains is observed compared to the other cases explained before. The longitudinal and lateral strains after 383 days of exposure are 2000 $\mu\varepsilon$ and 8000 $\mu\varepsilon$, respectively. The results indicate that the position of the steel bars in the specimens has a significant influence on the surface strains. The nearer the longitudinal steel bar to the concrete surface, the less the longitudinal strain. The ratio of the lateral to longitudinal strain is stabilized at around 4, which is the highest compared to the other cases explained before (**Fig. 9**).

Case 8

In this ASR case, in addition to the four corner reinforcements as in Case 7, five stirrups (6 mm diameter) were embedded in the specimens to limit the lateral strains. Compared to Case 7, a slight reduction in lateral strain is observed. However, the longitudinal strain is almost the same as Case 7. The ratio of the lateral to longitudinal strain is stabilized at around 3.4, which is lower than Case 7 (**Fig. 9**).

From the surface strain data of ASR specimens, it is clearly realized that before cracking the rate of expansion is slow, and after cracking it increased rapidly, and finally almost stabilized. From these results, the expansion process is divided into incubation period with a slow rate of expansion, cracking period with a rapid rate of expansion, and finally a stabilized period without any significant expansion. Pulse velocity, compressive strength, and Young's modulus data also show the same trend as explained before. The same process of strain development over the steel bars in concrete is also observed. These data are explained in the next section.

3.3 Strain Over the Steel Bars Embedded in Concrete

Average strain over the steel bar in each specimen is explained in this section. Cases 1 and 2 were made without reinforcement, therefore, the explanation begins from Case 3. The average strain over the steel bar for each case is shown in **Fig. 10**. The average strain of a specimen represents the average strains obtained from the strain gages embedded in each specimen (5 gages for each specimen for Cases 3~6, and 12 gages for each specimen for Cases 7 and 8). The average strain of each case represents the average strain of three specimens. For Case 8, two strain gages were also fastened over the mid stirrup, one on the vertical leg and one on the horizontal leg. The average strain of these strain gages is defined as the average strain over the stirrup of a specimen. Again, average strain of three specimens means average strain over the stirrup of Case 8.

Case 3

After cracking at around 65 days exposure, the

strain over the steel bars quickly increased and stabilized at around 1500 $\mu\varepsilon$ for a certain period and then decreased to the level of 1200 $\mu\varepsilon$. The reduction of the strain over the steel bar cannot be explained. However, it is expected due to the leaching of the alkali-silica gel from concrete, and therefore reducing the force induced by the expansion. Relevant data on this matter are explained later.

Case 4

The strain over the steel bars dramatically decreased compared to Case 3. The strain over the bar is stabilized at around 500 $\mu\varepsilon$ for a certain period and later decreased as in Case 3. The results indicate that with the absence of the end plates, the degree of restraint provided by the steel bars in concrete decreases and concrete is allowed to expand more freely.

Case 5

The strain over the steel bars is stabilized at around 1250 $\mu\varepsilon$ for a certain period, which is lower than Case 3, but higher than Case 4. It is supposed due to the greater restraint provided by the deformation over the deformed bar compared to Case 4 with plain bar. The degree of restraint for Case 5 will be less than Case 3 with end plates. The results strongly indicate that ASR induced strains will depend on the restraint provided by the steel bars in concrete.

Case 6

The strain over the steel bars is stabilized at around 750 $\mu\varepsilon$ for a certain period, which is about half of the stabilized strain of Case 3. The steel area in Case 6 was about 3.7 times higher than Case 3, however the strain over the steel bar for Case 6 is about half of Case 3. No significant difference in the surface strains is observed with the variation of the amount of steel bars as explained in the previous section (**Figs.** 7 and **8**). It is supposed due to the lower restraint provided by the end plates of Case 6. The size of the end plates for Case 3 and 6 was the same but the diameter of the bar was double of Case 6 compared to Case 3. It is important to note that a 25 mm round bar was not available in the market, therefore, larger deformed bars were polished to make 25 mm round bars. The size of the end plates was also the same for all cases. Compared to Case 3, the large diameter of Case 6 leads to a relatively small area at the end to provide the restraint. It is expected that the smooth steel surface as well as less effective plate area at the ends of the bar cause to generate more slip over the bar.

Case 7

The strain over the steel bars stabilized at around 1400 $\mu\varepsilon$ for a certain period. The amount was almost the same as Case 3, where only one steel bar was embedded at the center with end plates. It is also important to note that in Case 7, the total amount of longitudinal steel area was kept similar to Case 6. However, the strain over the steel bars was higher for Case 7 compared to Case 6. The surface strain was already discussed in the previous section. The results strongly support the influence of the location of the steel bars on the strain development over the bar, and also over the surface as explained before. The strain over the bar near the surface is higher than the bar far from the surface.

Case 8

Compared to Case 7 no significant change in the strain over the steel bars is observed with the addition of the stirrups in the specimens.

The strain over the legs of the stirrup is higher than the longitudinal strain over the main steel bars. The strain over the stirrup becomes 2000 $\mu\varepsilon$ after 383 days of exposure, which is higher than the yield strain of the steel bars. Relatively higher lateral surface strain compared to the longitudinal surface strain leads to the generation of higher strain over the stirrup.

From the results explained in this section, it is also realized that the strain over the steel bars increases slowly at the early stage of exposure, then it rapidly increases after cracking and finally stabilizes for a certain period. Therefore, it is understood that the strain development over the steel bars closely follows the three stages of ASR expansion, i.e., the incubation period, the cracking period, and the stabilized period. It is also important to note that a reduction in strain over the steel bars is observed after a certain stabilized period, which is supposed due to the leaching of ASR

gel from the specimens. For large specimens, and also specimens not exposed to seawater, this phenomenon may not be observed. Therefore, it is recommended to carry out additional investigation on large cube specimens. Relevant data on the leaching of gel is explained later. Slip over the steel bars may also influence the results.

Table 6 Average Crack Widths (Laterals Cracks) and Depths (at 303 Days of Exposure)

Case	Crack Widths (mm)	Crack Depths (mm)
2	0.172	12.90
3	0.100	8.64
4	0.130	12.20
5	0.110	11.55
6	0.100	11.40
7	0.100	9.10
8	0.100	8.57

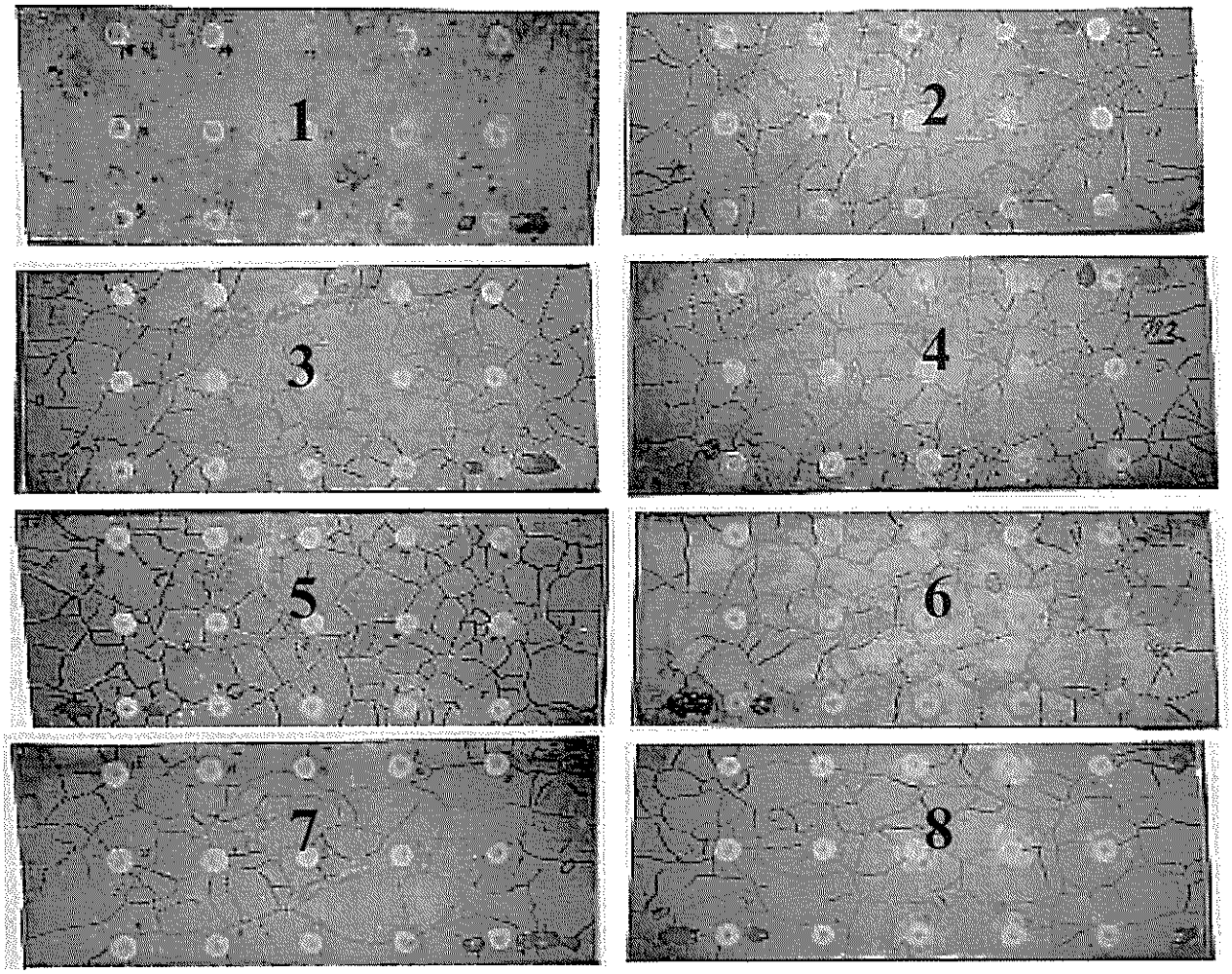

At 383 Days of Exposure

Fig. 11 Crack Maps Over the Specimens at 383 Days of Exposure

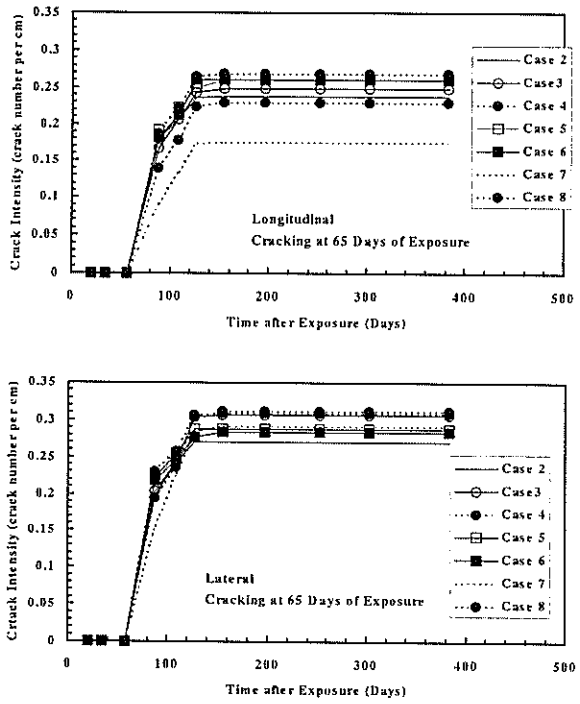

Fig. 12 Crack Intensity Over the Specimens

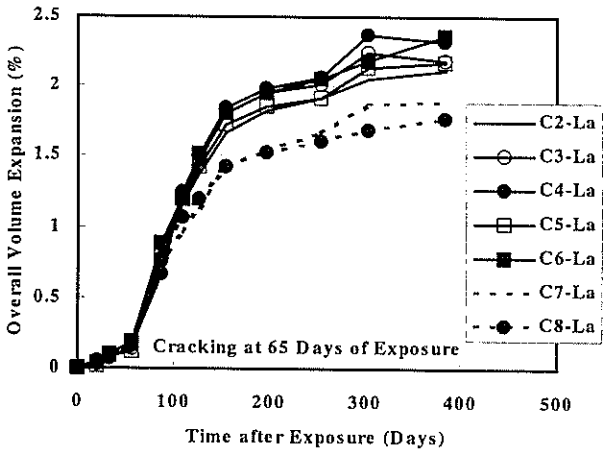

Fig. 13 Volume Change of the Specimens

3.4 Crack Maps, Crack Intensity, Crack Widths and Depths, and Overall Volume Expansion

Crack maps over the surface of the specimens are shown in **Fig. 11** for all of the cases after 383 days of exposure. Only one specimen per case is shown. Fewer lateral cracks were found for Cases 7 and 8. It is expected due to the placement of the steel bars near the surface of the specimens. A significant amount of strain in the lateral direction causes the cracks to run mostly in the longitudinal direction for Cases 7 and 8. No significant difference in the crack patterns is observed in other cases. Crack intensity over the specimens in the lateral and longitudinal directions is shown in **Fig. 12**. Crack intensity is defined as the number of cracks per unit cm of the specimens in the lateral or longitudinal direction. It is found that crack intensity increases rapidly at the beginning of the cracking and later no significant increase is found. The crack intensity in the longitudinal direction was lower for Cases 7 and 8 compared to the others. It is due to the significant amount of restraint provided by the steel bars at the corners of the beams. A tendency of higher crack intensity in the lateral direction is also found for Cases 7 and 8. It is expected due to the significant amount of strain in the lateral direction, which helps to generate the cracks in the longitudinal direction.

The change in the crack widths was observed in the cracking period with the development of a few additional new cracks. The crack width was stabilized later. New cracks were also not developed in the stabilized period. Relatively lower crack widths were observed for Cases 7 and 8 compared to the other cases made with reactive aggregate.

Crack widths (lateral direction) and depths in the longitudinal directions were measured after cutting the specimens in the longitudinal directions. The average crack widths and depths are summarized in **Table 6**. No difference in the average crack widths is observed between Cases 3, 6, 7, and 8. Relatively wider cracks were observed for Cases 2, 4, and 5. No steel bars are provided in Case 2, therefore it is free to expand, which causes the generation of wider cracks. The less restraint provided by the steel bars for Cases 4 and 5 also results in wider cracks. Relatively larger crack depths were also observed for the cases with wider crack widths. The depths of the surface cracks were limited over a thin surface region surrounding the specimens. For this reason, the chloride penetration is also limited to the surface region only. These data are explained later.

The overall volume expansion of the specimens is shown in **Fig. 13**. The volume expansion was calculated based on the lateral and longitudinal surface strains over the specimens. It is found that the volume expansion is reduced with the improvement of restraint conditions.

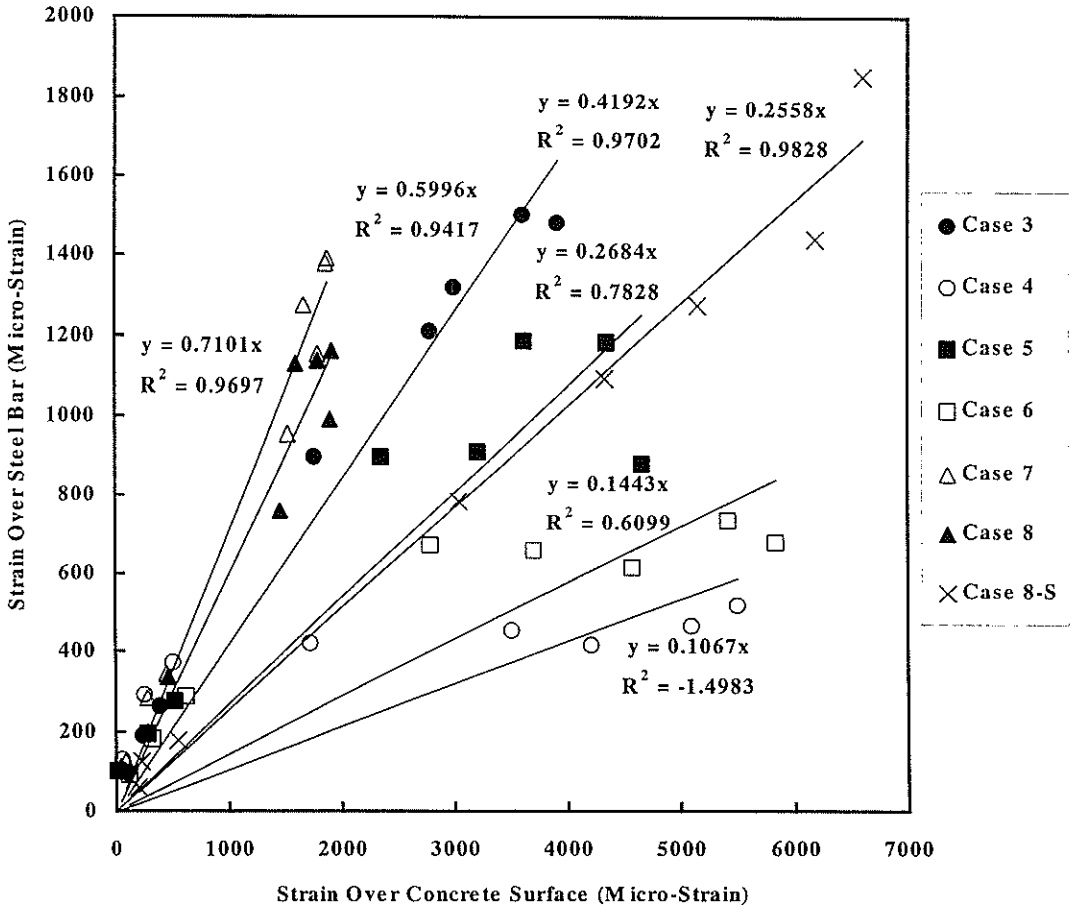

Fig. 14 Surface Strain and Strain Over the Steel Bars

3.5 Relationships Between Surface Strain and Strain Over the Steel Bar

To predict the relationships between the surface strain and the strain over the steel bars, the data until the age of 198 days were used. After 198 days, in many cases it was found that the strain over the steel bars decreased. Inclusion of these data causes a poor relation between the surface strain and strain over the steel bars. The variation of strain over the steel bars and corresponding surface strain is shown in **Fig. 14** until the age of 198 days. Linear relationship for each case is also shown in the same figure with R-squared value. The linear relations are given below for Cases 3~8:

Case 3	$\varepsilon_{st} = 0.42\,\varepsilon_{con}$	$R^2 = 0.97$	(3)
Case 4	$\varepsilon_{st} = 0.1067\,\varepsilon_{con}$	$R^2 = -1.5$	(4)
Case 5	$\varepsilon_{st} = 0.2684\,\varepsilon_{con}$	$R^2 = 0.78$	(5)
Case 6	$\varepsilon_{st} = 0.144\,\varepsilon_{con}$	$R^2 = 0.61$	(6)
Case 7	$\varepsilon_{st} = 0.7101\,\varepsilon_{con}$	$R^2 = 0.97$	(7)
Case 8	$\varepsilon_{st} = 0.6\,\varepsilon_{con}$	$R^2 = 0.94$	(8)
Case 8 - Stirrup	$\varepsilon_{st} = 0.2558\,\varepsilon_{con}$	$R^2 = 0.98$	(9)

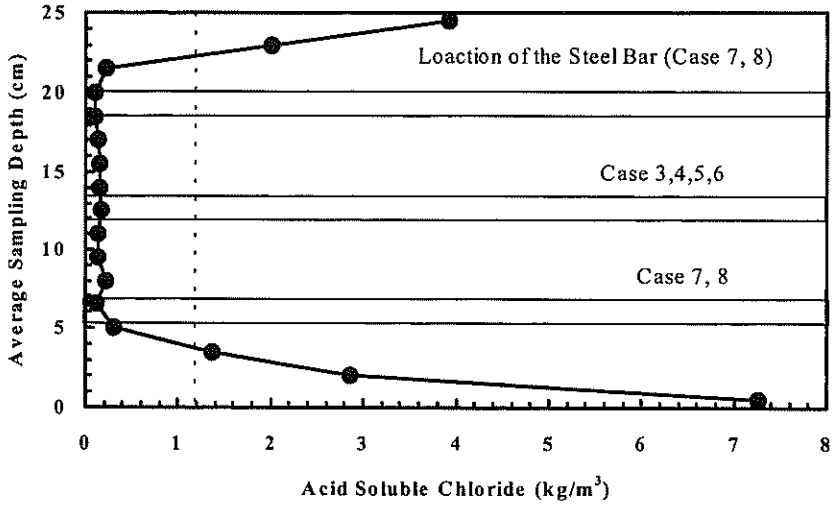

Fig. 15 Chloride Profile Across the Specimen (Case 2)

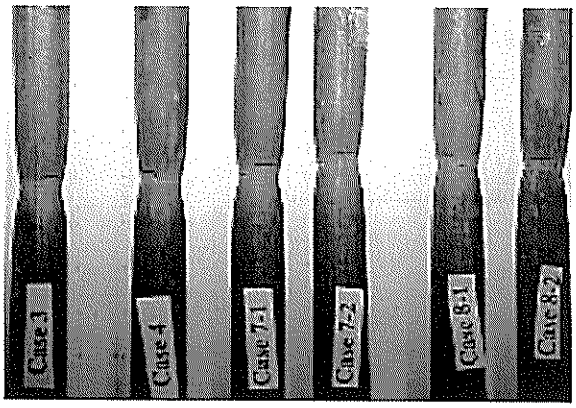

Fig. 16 Neck Formation At Failure During Tensile Tests

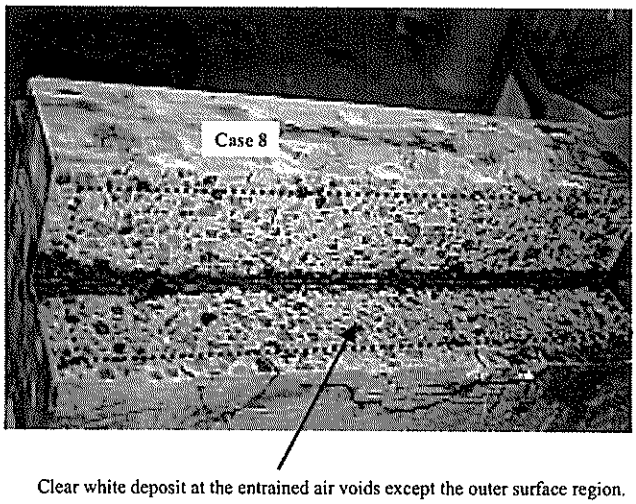

Fig. 17 Autopsied Specimen (Case 8)

For Case 4, a significant amount of slip over the steel bars causes a poor linear relation. For Cases 5 and 6, the relationship also becomes relatively poor for the same reason. Based on the experimental results, the following linear relations are proposed for the prediction of strain over the steel bars based on the measured surface strain over the specimens:

$$\varepsilon_{st} = \beta \varepsilon_{con} \qquad (10)$$

The factor β depends on the internal restraint provided by the steel bars inside the specimens as well as the location of the bars inside the specimens as explained earlier.

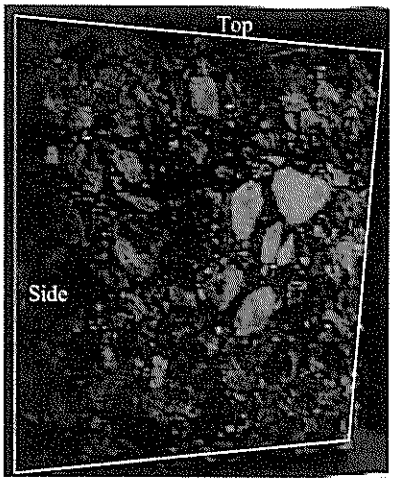

10 x 10 cm Surface

Fig. 18 Cut Surface After Treated with Uranyl Acetate Solution

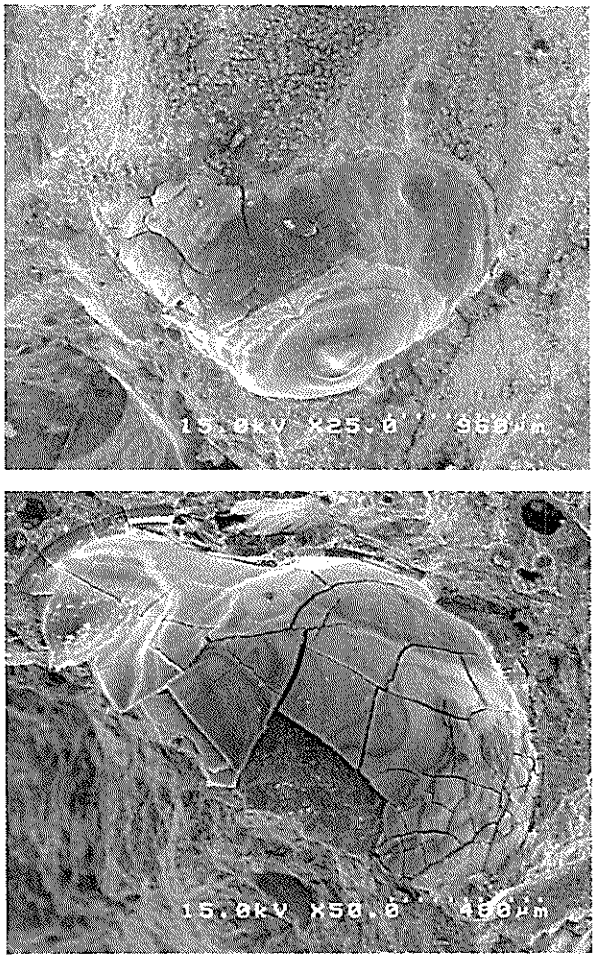

Top: 5 ~ 15 mm from the surface

Bottom: 65 ~ 75 mm from the surface

Fig. 19 Voids in Concrete Filled with ASR Gel (Cracks due to the water loss)

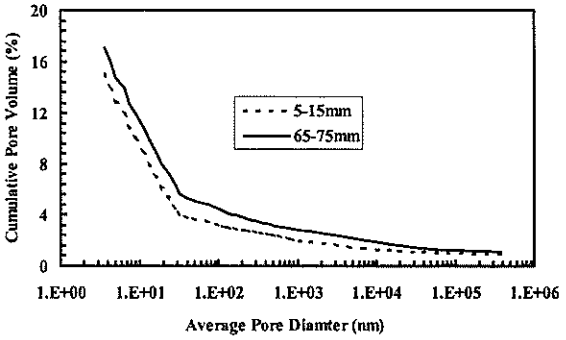

Fig. 20 Pore Volume at the Inner and Outer Regions

3.6 Others

The chloride profile in the specimens at 303 days of exposure is shown in **Fig. 15**. It is found that the chloride level over the steel bar is lower than the chloride threshold level. The chloride threshold level is considered to be 1.2 kg/m^3 (**17**). After collecting the steel bars from the specimens, no trace of corrosion over the steel bars (main steel bars or steel bars) was found. The same investigation on the remaining specimens will be carried out in the future. The authors investigated the corrosion of steel bars in concrete to check the influence of high alkalinity of concrete. Another particular interest was if corrosion occurs how it will proceed in a highly stressed steel bar (induced by ASR). The mechanical properties of the steel bars were tested after 303 days of exposure. No significant change in mechanical properties (yield stress, ultimate stress, and percentage of elongation) of the steel bars was observed. The failure location of the steel bars is shown in **Fig. 16**. Formation of a neck over the steel bars is observed. No significant difference in percentage of elongation, yield stress, and ultimate stress was found after and before exposure. The stress-strain curves of the steel bars after exposure also showed the clear strain hardening behavior after yielding.

ASR gels are clearly observed at the void regions by naked eye, especially at the inner regions of the specimens. An autopsied specimen is shown in **Fig. 17**. A clear white deposit of ASR gel was found at the inner region. However, it was not found at the surface region. It is due to the leaching of alkali from the surface region, lack of coarse aggregates near the surface, and also the leaching of ASR gel, if there is any. A 10x10

cm cut surface treated with uranyl acetate solution is shown in **Fig. 18**. No ASR gel is found near the surface region of the specimens. The microstructure of concrete was also checked after 303 days of exposure. The porosity of the mortar portion at the inner and outer regions of the specimens is shown in **Fig. 19**. It is found that the outer region becomes denser than the inner region. It is due to the deposition of Friedel's salt and ettringite at the outer region, which were confirmed by the XRD. SEM micrographs at the inner and outer regions of the specimens are also shown in **Fig. 20**. The presence of ASR gel is clearly found at the void region. However, the pore volume at the outer region is lower than the inner region as explained in **Fig. 19** due to the reduction in coarse pore volume. The cracks are developed due to the water loss from the gel. No significant change in the microstructure of the hardened matrix was also noted based on the SEM investigation at the inner and outer regions of the specimens.

3.7 Future Investigations

Investigations are still continuing on the surface strain of the specimens. Unfortunately, many strain gages became inactive and future recording of data on the strain over the steel bars will not be possible. The authors are still trying to propose a suitable structural model for FEM analysis of the beam specimens subjected to ASR expansion.

The author strongly recommend investigation on the large blocks confined with different steel ratios in order to understand the brittle failure of the steel bars due to the ASR expansion. Based on the investigation on this study, it is easily realized that ASR can induce a tremendous stress over the steel bars in concrete. It will largely depend on the size of the specimens.

4. Conclusions

Based on the scope of this study, the following conclusions are drawn:

1. Young's modulus of concrete drops significantly due to the ASR in concrete, especially immediately after cracking. However, it becomes stable later. Fortunately, the reduction in compressive strength was not as significant as Young's modulus.
2. Expansion over concrete surface induced by ASR is divided into three periods, such as the incubation period, cracking period, and stabilized period.
3. Internal restraint provided by the steel bars results in the reduction of surface strain in the restraint direction. The degree of restraint has a significant influence on the surface strain as well as strain over the bars.
4. A good linear relation between the surface strain and the strain over the steel bars is found, especially for the cases with highly restrained conditions. The proposed linear relations can be used to predict the strain over the steel bars.
5. Less surface strain is observed if the steel bars are placed near the concrete surface, however, the strain over the bars is increased for this arrangement. Placing longitudinal steel bars near the surface also results in the significant lateral surface strain as well as higher strain over the stirrups, if any. Placing the stirrups causes a slight reduction in strain in the lateral direction.

(Received on February 14, 2003)

Acknowledgements

The authors wish to express their gratitude and sincere appreciation to the authority of *Port and Airport Research Institute, Independent Administrative Institution, Japan* for giving support to perform this study. The authors also thankful to Ms. Madoka Satoh of Materials Division, Port and Airport Research Institute for her help during the experimental process.

References

1. Fournier Benoit and Berube Marc-Andre, Alkali-aggregate Reaction in Concrete: A Review of Basic Concepts and Engineering

Implications, Canadian Journal of Civil Engineering, Vol. 27, 2000, pp. 167-191.

2. Shenfu, Fan, and Hanson, John, M., Length Expansion and Cracking of Plain and Reinforced Concrete Prisms Due to Alkali-Silica Reaction, ACI Materials Journal, Vol. 95, No. 4, July – August 1998, pp. 480-487.
3. Zhang, C., Wang, A., Tang, M., Zhang, N., Influence of Dimension of Test Specimens on Alkali-Aggregate Reactive Expansion, ACI Materials Journal, Vo. 96, No. 2, March-April 1999, pp. 204-207.
4. Prezzi, M., Monterio, P.J.M., and Sposito, G., Alkali-Silica Reaction – Part 2 : The Effect of Chemical Admixtures, ACI Materials Journal, Vol. 95, No. 1, January – February 1998, pp.3-10.
5. Prezzi, M., Monterio, P.J.M., and Sposito, G., Alkali-Silica Reaction – Part I : Use of Double-Layer Theory to Explain the Behavior of the Reaction Product Gels, ACI Materials Journal, Vol. 94, No. 1, January – February 1997, pp. 10-17.
6. RILEM TC 106-AAR: Aggregates for Alkali-Aggregate Reaction – International Assessment of Aggregates for Alkali-Aggregate Reactivity, Materials and Structures, Vol. 33, March 2000, pp. 88-93.
7. Ahmed, T., Burley, E., Rigden, S., The Static and Fatigue Strength of Reinforced Concrete Beams Affected by Alkali-Silica Reaction, ACI Materials Journal, Vol. 95, No. 4, July – August 1998, pp. 376-388.
8. Ahmed, T., Burley, E., Rigden, S., Effect of Alkali-Silica Reaction on Bearing Capacity of Plain and Reinforced Concrete, ACI Structural Journal, Vol. 96, No. 4, July-August 1999, pp. 557-570.
9. Ahmed, T., Burley, E., Rigden, S., Effect of Alkali-Silica Reaction on Tensile Bond Strength of Reinforcement in Concrete Tested under Static and Fatigue Loading, ACI Materials Journal, Vol. 96, No. 4, July – August 1999, pp. 419-428.
10. Thaulow, N., Hjorth, U.J., and Clark B., Composition of Alkali Silica Gel and Ettringite in Concrete Railroad Ties: SEM-EDX and X-Ray Diffraction Analyses, Cement and Concrete Research, Vol. 26, No. 2, pp. 309-318, 1996.
11. Diamond, S., ASR – Another Look at Mechanisms, In Proceedings of the Eight International Conference on Alkali Aggregate Reaction in Concrete, Kyoto, Japan, Ed. Okada, K., Nishibayashi, S., and Kawamura, M., pp. 83-94, 1989.
12. Kagimoto, H., Sato, M., and Kawamura, M, Evaluation of Degree of ASR Deterioration in Concrete and Analysis of Pore Solutions, Concrete Library of JSCE, No. 36, pp. 281-293, February 2000.
13. Kubo, Y., Iketomi, O., Nakashima, T., and Torii, K., Experimental Study of Fracture of Reinforced Steel Bar in Concrete Structures due to Alkali-Silica Expansion, Sixth CANMET/ACI International Conference on Durability of Concrete, Greece, June 2003 (submitted, collected by personal communication).
14. Sims, I., Alkali-Silica-Reaction – UK Experience, In Book "The Alkali-Silica Reaction in Concrete, Ed. Swamy, R.N., Blackie, Glasgow and London, U.K., New York, USA, 1990.
15. Guide to Durable Concrete, Reported by ACI Committee 201, ACI 201.2R-01, October 2001, pp. 26.
16. Mohammed, T.U., Hamada, H., and Yamaji, T., ASR Induced Strains Over Concrete Surface and Steel Bars in Concrete, ACI Materials Journal (accepted).
17. Japan Society of Civil Engineers: Standard specification for concrete, maintenance, 2001.